EXCITED ELECTRON PRODUCTION AT THE SPPC-BASED *ep* COLLIDERS VIA CONTACT INTERACTIONS*

A. Caliskan

Gümüşhane University, Faculty of Engineering and Natural Sciences
Department of Physics Engineering
29100, Gümüşhane, Türkiye
acaliskan@gumushane.edu.tr

Received 6 May 2024, accepted 5 June 2025,
published online 23 June 2025

If a linear electron accelerator is installed into the SPPC (Super Proton–Proton Collider) complex, *ep* collision options will be available in addition to *pp* collisions. We consider the production of excited electrons with spin-1/2 at the future SPPC-based electron–proton colliders with center-of-mass energies of 8.44, 11.66, 26.68, and 36.88 TeV. In the $ep \to e^{\star}X \to e\gamma X$ signal process, excited electrons are produced by contact interactions and decay into the photon channel by gauge interactions. Taking into account the corresponding background process, the pseudorapidity and transverse momentum distributions of the final-state particles are plotted. We reported on the discovery, observation, and exclusion mass limits of excited electrons by applying appropriate kinematical cuts best suited for amplifying the signal of the excited electron signature. We also investigated the highest achievable values of the compositeness scale for the discovery of excited electrons at these colliders.

DOI:10.5506/APhysPolB.56.7-A1

1. Introduction

The Standard Model (SM) in particle physics is a fundamental theory that successfully describes the basic particles and three of the four fundamental interactions between these particles. In 2012, the discovery of the Higgs boson at CERN by the ATLAS [1] and CMS [2] detectors confirmed the Electroweak Symmetry Breaking mechanism proposed by the SM. With this discovery, which is a milestone in particle physics, the mechanism of gaining mass to particles has been experimentally proven. Although all the experiments performed so far have confirmed the SM, there are many phenomena that this theory has not yet been able to explain, such as dark matter, dark energy, elementary particle inflation, family replication, and CP violation. In order to provide a theoretical solution to these problems, various theories such as Technicolour [3, 4], Grand Unified Models [5, 6], Supersymmetry [7], Extra Dimensions and Compositeness [8] have been proposed. This study has been conducted within the scope of compositeness theory, as the compositeness can provide a particularly good explanation for the fundamental particle inflation. In these models, the existence of more fundamental particles called preons has been proposed. All fermions and their anti-particles are composed of bound states of the preons. The first studies on the lepton and quark compositeness began in the 1970s [9–12]. Up to date, numerous preonic models such as Haplon (Fritzsch–Mandelbaum) [13, 14] and Rishon (Harari–Shupe) [15, 16] have been proposed, suggesting new particles such as excited fermions, leptogluons, and leptoquarks within the scope of these models. According to preonic models, possible new interactions between fermions occur on the binding energy scale of the preons. This energy scale, where preons come together to form SM fermions, is called the compositeness scale and is denoted by Λ. If the leptons and quarks in the SM have a composite structure, their excited states should be observed experimentally as a requirement of compositeness. Therefore, excited leptons and quarks are among the proposed new particles. The masses of these proposed particles are expected to be heavier than their SM counterparts.

In the literature, many studies on excited leptons [17–22] and quarks [23–25] have been carried out for various colliders. In this study, single production of excited electron by a contact interaction method is investigated. It is a continuation of our previous work [26] in which the production by gauge mechanism was investigated. No signal for the existence of excited leptons has been found in experimental studies. However, each new study updates the experimental mass limits of excited leptons. The most recent mass limits for single production of excited electrons are 3.9 TeV for gauge decay [27, 28] and 5.6 TeV for contact decay [29]. Since the decay of excited electrons by gauge interactions is considered in this study, the mass limit of 3.9 TeV is taken into account. This mass limit is provided by the CMS detector for the $pp \to ee^{\star}X \to ee\gamma X$ process, assuming $f = f' = 1$ and $\Lambda = m_{e^{\star}}$.

In this study, the production of excited electrons by contact interactions and their decay by the gauge mechanism were investigated in the SPPC-based electron–proton collider, which is proposed to be established in China. The rest of the paper is organised as follows: Section 2 describes the SPPC-CEPC project and the proposed electron–proton collider options, Section 3 discusses the Lagrangian, decay width, and cross sections of excited leptons, Section 4 performs the signal–background analysis, and Section 5 interprets the results obtained.

2. The SPPC project and electron–proton colliders

Particle physics has reached the Higgs era with the definitive proof of the existence of the Higgs particle in experiments conducted at CERN. In order to further our knowledge on this subject, the properties of the Higgs particle need to be analysed in more detail. For this purpose, efforts to establish Higgs factories to produce the Higgs particle at higher energies have been initiated all over the world. Thanks to the Higgs factories, more information about the Higgs field will be obtained by carrying out studies on topics such as the precise measurement of the Higgs mass and the observation of rare decay products. Studies on new particles and interactions beyond the SM will also be carried out at these factories.

Just a few months after the discovery of the Higgs particle, the Chinese Particle Physics Community proposed the two-stage CEPC-SPPC project. In the first phase of the project, an electron–positron collider named Circular Electron Positron Collider (CEPC) will be installed. The CEPC collider to be built in China will have a tunnel length of approximately 100 km, where electron and positron beams travelling in opposite directions will be collided in detectors to be installed at two points [30, 31]. The center-of-mass energies of the collider are targeted to be 91, 160, and 240 GeV with corresponding luminosities of 32, 10, and $3 \times 10^{34}\,\mathrm{cm}^{-2}\mathrm{s}^{-1}$, respectively. Since the main purpose of the collider is to investigate the properties of the Higgs particle, it will work as a Higgs factory for the first 7 years and it is expected to produce at least 1 million Higgs particles during this process. In the next few years, it is planned to produce 1 trillion Z bosons in 2 years as a super Z factory and 100 million W bosons in 1 year as a W factory. In the second phase of the project, a proton–proton collider, the Super Proton–Proton Collider (SPPC), will be built as an energy frontier and a discovery machine beyond the LHC [32].

At the SPPC collider, which will share the same tunnel with the CEPC collider, the goal in the first stage will be to reach a center-of-mass energy of 70–75 TeV with dipole magnets of 12 T. The SPPC, which is expected to reach a luminosity of $1 \times 10^{35}\,\mathrm{cm}^{-2}\mathrm{s}^{-1}$, will be a more powerful pp collider than the LHC at CERN with these values. At the next stage of the project, it is planned to increase the center-of-mass energy of the SPPC collider to energies of 125–150 TeV by using 20 T dipole magnets. With these energy values, the SPPC collider will be more powerful than the 100 TeV pp collider in the FCC project [33–36]. The SPPC collider is planned to be installed after 2040 [37]. The Preliminary Content Design Report (Pre-CDR) of the CEPC-SPPC project was written in 2015 [38] and the Content Design Report (CDR) in 2018 [39, 40]. The Technical Design Report (TDR) of the project is still in progress and is expected to be finalised in the coming months.

The installation of the CEPC and SPPC colliders in the same tunnel will enable the ep collision option in addition to pp and ee^+ collisions. As a result of a preliminary study on this subject, parameters $\sqrt{s} = 4.1$ TeV and $L_{ep} = 10^{33}\,\mathrm{cm}^{-2}\mathrm{s}^{-1}$ were obtained [41]. It can be seen that the center-of-mass energy is quite small here, because the problem of synchrotron radiation in circular electron accelerators prevents reaching high energies. If a linear electron accelerator is used instead of a circular one, an ep collider with a higher center-of-mass energy can be obtained. In another study in this direction, a linear electron accelerator tangential to the SPPC proton ring was proposed and the basic parameters for the ep option were derived [42]. Higher center-of-mass energies were achieved in this study, which used the parameters of the ILC and PWFALC linear electron accelerator projects as the electron source. For the proton energy, two options were used: 35.6 TeV, an energy value that can be reached in the first stage of SPPC, and 68 TeV, that can be reached in the second stage. Thus, four different ep collision options were derived. These parameters are given in Table 1.

Table 1. The main parameters of the SPPC-based electron–proton colliders.

E_e [TeV]	E_p [TeV]	$\sqrt{s}$ [TeV]	L_{int} [$\mathrm{cm}^{-2}\mathrm{s}^{-1}$]
0.5	35.6	8.44	2.51×10^{31}
0.5	68	11.66	6.45×10^{31}
5	35.6	26.68	7.37×10^{30}
5	68	36.88	1.89×10^{31}

3. Gauge and contact interactions for excited electrons

Both the production and decay processes of excited leptons in colliders can take place through two different interaction mechanisms. If the interaction between particles is realised by the exchange of specific particles, this interaction is defined as a gauge interaction. The gauge interaction Lagrangian between spin-1/2 excited leptons, ordinary leptons, and gauge bosons is given as [43, 44]

$$L_{\mathrm{gauge}} = \frac{1}{2\Lambda}\bar{L}_{\mathrm{R}}^{\star}\sigma^{\mu\nu}\left[fg\frac{\vec{\tau}}{2}\cdot\vec{W}_{\mu\nu} + f'g'\frac{Y}{2}B_{\mu\nu}\right]L_{\mathrm{L}} + \mathrm{h.c.}\,, \tag{1}$$

where $L_{\rm L}$ and $L^{\star}_{\rm R}$ denote left-handed ordinary lepton and right-handed excited lepton, respectively, $\vec{W}_{\mu\nu}$ and $B_{\mu\nu}$ are the field strength tensors, Λ is the compositeness scale, f and f' are the scaling factors, g and g' are the gauge couplings, Y is hypercharge, $\sigma^{\mu\nu} = i(\gamma^{\mu}\gamma^{\nu} - \gamma^{\nu}\gamma^{\mu})/2$, where γ^{μ} are the Dirac matrices, and $\vec{\tau}$ represents the Pauli matrices.

The other interaction mechanism of excited leptons is four-fermion contact interactions which are effective at short distances. The effective Lagrangian describing this interaction is given in equation (2) [43, 44]

$$L_{\rm contact} = \frac{g_{\star}^2}{\Lambda^2}\frac{1}{2}j^{\mu}j_{\mu}\,, \tag{2}$$

$$j_{\mu} = \eta_L \bar{f}_{\rm L}\gamma_{\mu}f_{\rm L} + \eta'_{\rm L}\bar{f}^{\star}_{\rm L}\gamma_{\mu}f^{\star}_{\rm L} + \eta''{}_{\rm L}\bar{f}^{\star}_{\rm L}\gamma_{\mu}f_{\rm L} + {\rm h.c.} + (L \to R)\,. \tag{3}$$

In equations (2) and (3), $g_{\star}$ is the interaction constant and its value is $g_{\star}^2 = 4\pi$. Λ is the compositeness scale and j_{μ} represents the left-handed currents. η factors are the coefficients of these left-handed currents and their value is taken as 1. f and $f^{\star}$ are the SM and the excited fermion fields, respectively.

When we analyse both Lagrangians, it is seen that the compositeness scale, Λ, is inversely proportional. Therefore, it is clearly seen that as the Λ increases for both interactions, the cross section and decay width values will decrease. However, while the Lagrangian is inversely proportional to Λ in the gauge interaction, it is inversely proportional to Λ^2 in the contact interaction. This means that gauge interactions dominate at high-Λ values and contact interactions dominate at low-Λ values. In this study, since the excited electrons will be produced with the $e,p \to e^{\star}, j$ process by the contact interaction method, we set Λ equal to the mass of the excited electron, $\Lambda = m_{e^{\star}}$. Thus, we obtained both a high cross section and a situation in which the contact interaction is dominant.

Excited electrons can decay by both mechanisms. There are three decay modes for gauge interactions. These are $e^{\star} \to e\gamma$, $e^{\star} \to eZ$, and $e^{\star} \to \nu W^-$ decay channels. If we neglect the SM quark masses and for the $m^{\star} > m_{W,Z}$ condition, the analytical formulae giving the decay width of these channels are given in equation (4)

$$\Gamma(l^{\star} \to lV) = \frac{\alpha m^{\star 3}}{4\Lambda^2} f_V^2 \left(1 - \frac{m_V^2}{m^{\star 2}}\right)^2 \left(1 + \frac{m_V^2}{2m^{\star 2}}\right)\,, \tag{4}$$

where V represents the γ, Z, and $W^{\pm}$ bosons. $m^{\star}$ is the mass of the excited electron and m_v is the mass of the gauge boson. f_V is the interaction constant and its expression for each decay channel is given in equation (5)

$$\begin{aligned} f_\gamma &= fT_3 + f'\frac{Y}{2}\,, \\ f_Z &= fT_3\cos^2\theta_{\rm W} - f'\frac{Y}{2}\sin^2\theta_{\rm W}\,, \\ f_W &= \frac{f}{\sqrt{2}}\,, \end{aligned} \tag{5}$$

where T_3 is the third component of the weak isospin, Y is the hypercharge, and $\theta_{\rm W}$ is the weak mixing angle. For excited electrons, $T_3 = -\frac{1}{2}$ and $Y = -1$.

Three decay channels are also available for contact interactions. These are the $e^\star \to eq\bar{q}$, $e^\star \to e^-e^-e^+$, and $e^\star \to e\nu\bar{\nu}$ processes, where q represents quarks. The analytical formula for the decay width of these processes is given in equation (6)

$$\varGamma\left(l^\star \to lF\bar{F}\right) = \frac{m_l^\star}{96\pi}\left(\frac{m_l^\star}{\varLambda}\right)^4 N_C' S'\,. \tag{6}$$

In this equation, F and l represent SM fermions and leptons, respectively. N_C' is the colour factor and has a value of 1 for leptons and 3 for quarks. S' is an additional combinatorical factor with a value of 1 if $f \neq l$, 4/3 for quarks, and 2 for leptons if $f = l$.

For numerical calculations, we implemented both Lagrangians given in equations (1) and (2) to the CalcHEP simulation package [45] with the help of LanHEP code [46], and created the model file for excited electrons. Since in this study we will use the case where $\varLambda$ is equal to $m_{e^\star}$, we calculated the partial decay widths of both interactions for $\varLambda = m_{e^\star}$. The results are shown in figure 1.

When this graph is analysed, it is clearly seen that the decay channels of the contact interaction are dominant. The $eq\bar{q}$ channel has the highest decay width values. If we take each of these decay channels and decay the heavy mass W and Z bosons in the final state, we obtain the following 6 possible processes for the ep collider:

$$e^-p^+ \to e^\star p \to e^-q\bar{q}j\,, \tag{7}$$
$$e^-p^+ \to e^\star p \to e^-e^-e^+j\,, \tag{8}$$
$$e^-p^+ \to e^\star p \to e^-\nu\bar{\nu}j\,, \tag{9}$$
$$e^-p^+ \to e^\star p \to W^-\nu j \to e^-\bar{\nu}\nu j\,, \tag{10}$$
$$e^-p^+ \to e^\star p \to e^-\gamma j\,, \tag{11}$$
$$e^-p^+ \to e^\star p \to e^-Zj \to e^-q\bar{q}j(e^-e^-e^+j)\,. \tag{12}$$

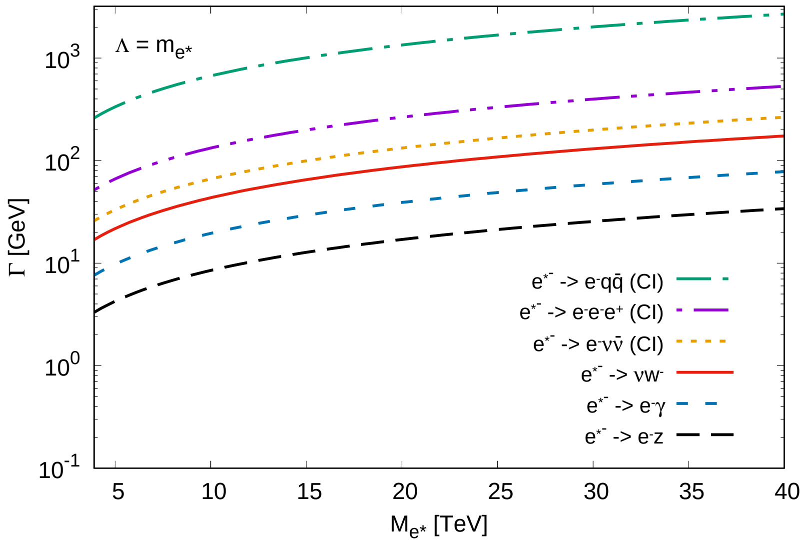

Fig. 1. The partial decay widths for both gauge and contact interactions of the excited electron for the energy scale of $\Lambda = m_{e^\star}$.

Since the photon channel has fewer final-state particles and is easier to observe in the detector, we chose this channel for the study. In addition, the photon channel was also used in the last experimental study conducted by the CMS group, where the most recent mass limits of excited leptons were determined. In this experimental study, excited leptons were produced by contact interactions and decayed by gauge interactions and the photon channel was chosen. Therefore, in this paper, we have taken exactly this experimental work as an example. In addition to the mass limits, the CMS group also obtained the most recent compositeness scale limit. For a 1 TeV excited lepton mass, the compositeness scale is excluded up to 25 TeV.

After selecting the photon decay channel, the cross-section values of the $ep \to e\gamma j$ process for the proposed 4 ep collider options were calculated for $\Lambda = m_{e^\star}$ and the results are shown in figure 2. As can be seen in these graphs, excited electrons are produced for both interactions and then decayed into the photon channel. Thus, we have compared both production mechanisms in these graphs. As it is clearly seen in all graphs, the contact production dominates over the gauge production for the $\Lambda = m_{e^\star}$ condition. On the other hand, considering the luminosity values in Table 1, these four colliders have the capacity to produce a sufficient number of events.

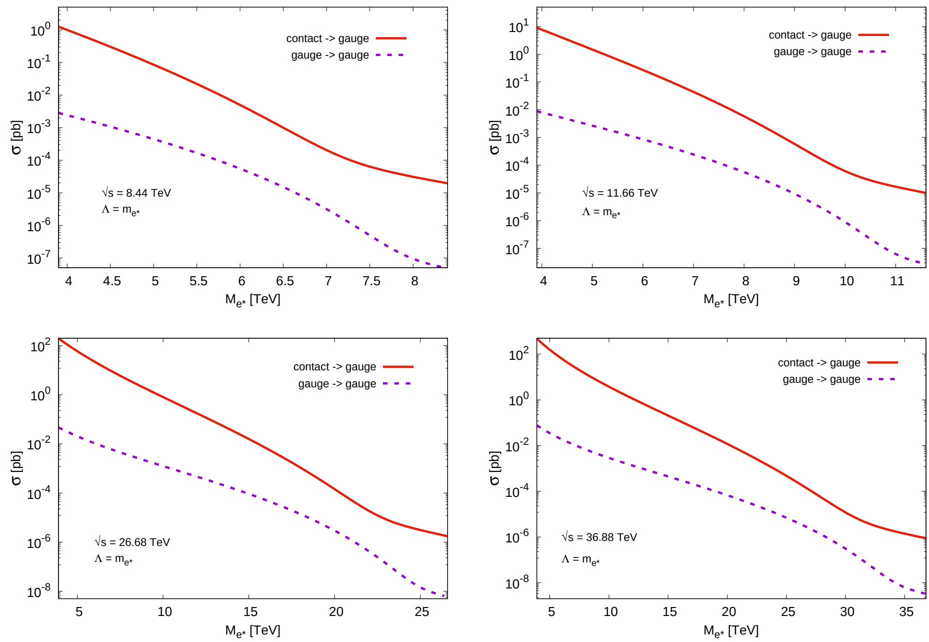

Fig. 2. The cross sections of the excited electrons for the both production mechanisms with respect to their mass at the SPPC-based electron–proton colliders with various center-of-mass energies for $\Lambda = m_{e^\star}$ and the coupling $f = f' = 1$.

4. Signal and background analysis

The SPPC-based ep colliders will enable us to search for excited electrons through the $ep \rightarrow e^\star j$ process (contact interaction), followed by the subsequent decay of the excited electrons into an electron and a photon (gauge decay). Therefore, our signal process is $ep \rightarrow e, \gamma, j$, where j represents jets and consists of quarks and antiquarks. The subprocesses of our signal are of the form of $eq(\bar{q}) \rightarrow e\gamma q(\bar{q})$, where q represents quarks and $\bar{q}$ represents antiquarks. The Feynman diagram of our signal process is shown in figure 3. In this work, we only consider tree-level diagrams corresponding to the lowest-order Feynman diagrams and do not include higher-order contributions such as loop-level diagrams or higher-order QCD corrections. The primary reason for this limitation is the computational constraints of the software tool used in this analysis, CalcHEP. It is known that higher-order contributions such as Next-to-Leading Order (NLO) can significantly change the results.

Since there are no studies in the literature that include higher-order contributions for excited electrons with contact interactions, it is quite difficult to estimate this contribution. However, we would like to briefly mention here

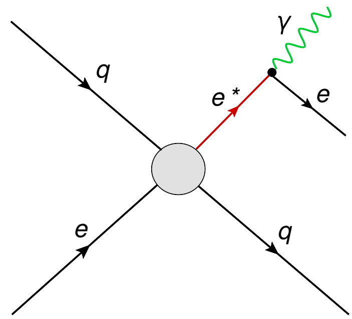

Fig. 3. Leading-order Feynman diagrams for the signal process $ep \to e^* j \to e, \gamma, j$.

as an example the QCD correction calculations made for some processes at the LHC collider. In a study of the effect of the NLO contribution on quark compositeness at the LHC, it was shown that exact NLO corrections suppress the New Physics signal compared to LO calculations and significantly lower the experimental limits. The CMS LO-based 4.0 TeV compositeness scale limit is reduced by 7.5% to 3.7 TeV with exact NLO, while the 3.4 TeV limit determined by ATLAS with the scaled NLO is reduced by 10% to 3.1 TeV with exact NLO calculations. Furthermore, in some kinematic regions, the LO and scaled NLO estimates overestimate the signal magnitude by up to 30% compared to the exact NLO [47]. In another study by the CMS Collaboration, possible deviations in the jet production cross section in proton–proton collisions ($\sqrt{s} = 7$ TeV) were investigated via the contact interactions (CI). Perturbative NLO level calculations were used for the SM quantum chromodynamics (QCD) background, which significantly reduced the theoretical uncertainties and provided excellent agreement with the measured jet P_{T} spectrum. In contrast, the contact interaction signal was modelled at the LO level; NLO corrections are estimated to change the CI limits by at most 5%, but are not included in this study. The NLO calculations increased the reliability of the background model due to the high sensitivity to the jet energy scale and particle distribution functions [48].

The background process corresponding to our signal is $ep \to e, \gamma, j$. All possible SM diagrams contributing to this process are given in figure 4. The q symbol in the eight Feynman diagrams seen in this graphic represents quarks. There are a total of 80 SM diagrams, 40 diagrams for $q = u, d, s, b, c$ quarks and 40 diagrams for their antiquarks.

In order to determine the Parton Distribution Function (PDF) that we will use in the simulations, a comparison of six distribution functions defined in the CalcHEP program was made. For this, the cross section of an excited electron with a mass of 4 TeV in the ep collider with a center-of-mass energy of 8.44 TeV was calculated separately for each distribution function. In this

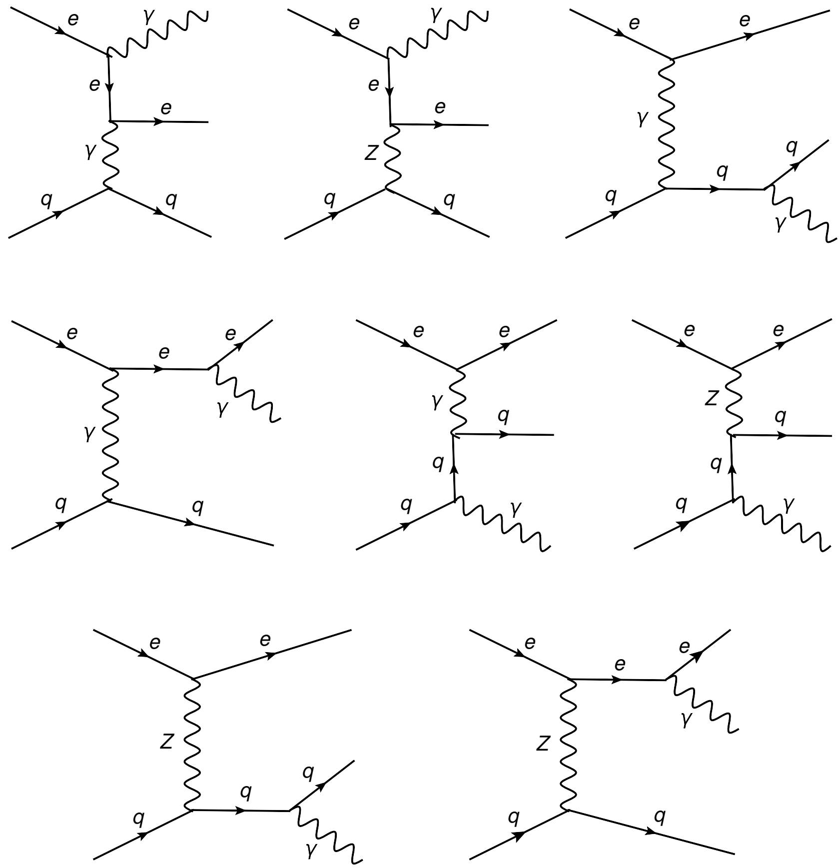

Fig. 4. The Feynman diagrams for the background process $ep \to e, \gamma, j$.

calculation for the signal process ($ep \to e^* j \to e, \gamma, j$) of the excited electron, 25 GeV pre-selection kinematical cuts were applied to the transverse momenta of the final-state particles, electrons, photons, and jets. The cross sections obtained for different PDF distributions of our signal process are reported in Table 2. The first column in Table 2 shows the code information of the PDF distributions, the second column shows the obtained cross-section values, and the third column shows the sensitivity in this calculation. According to these results, the PDF distributions give similar results with an average deviation of 1%. Therefore, using different PDF sets does not make any significant difference in terms of the accuracy of calculations. Therefore, the first-ranked CT10 distribution function was selected and used for our calculations [49].

Table 2. Cross sections of excited electron signal process ($ep \to e^*j \to e, \gamma, j$) obtained for different Parton Distribution Functions (PDF) and error rates in the calculations.

PDF	Cross sections [pb]	Errors [%]
CT10	0.999	0.00217
Cteq6l1	1.040	0.00256
NNPDF31_lo_as_0118	1.036	0.00236
PDF4LHC15_nlo_mc	0.989	0.00248
NNPDF23_lo_as_0130_qed	1.010	0.00238
NNPDF31_lo_as_0130	0.995	0.00248

4.1. Detector parameters

Since a detailed detector design for the SPPC-based *ep* colliders has not yet been carried out, the signal–background analysis is performed at the parton level. However, in this subsection, the sensitivity of today's detector technology in the measurement of some basic parameters will be briefly discussed. For this purpose, the parameters of the ATLAS detector of the High Luminosity LHC (HL-LHC) project [50], which is planned to be commissioned in 2029, are considered. The ATLAS detector is being upgraded to suit the operating conditions of the HL-LHC. For this purpose, the detector's Inner Tracker system will be completely replaced with a new silicon-only design. In this way, it is aimed at achieving a higher momentum resolution. In addition, the pseudorapidity values, which express the tracking range of the detector, will be extended from $|\eta| < 2.5$ to $|\eta| < 4$.

In this study, the final-state particles of our signal and background process are electrons, photons, and jets. Some important detector parameters of these particles are reconstruction, identification, isolation efficiency, energy scale, and momentum resolution. The systematic uncertainties for these parameters to be achieved at the HL-LHC are given in Table 3 [51].

According to the data in this table, it is understood that very high-precision measurements can be made. In a future *ep* detector, with the further development of technology, much more sensitive measurements will be possible.

Table 3. Representative systematic uncertainties in the measurement of some parameters of electron, photon, and jets at the HL-LHC.

Particles	Parameters	Range	Uncertainty [%]
Electron	Energy scale	$P_{\mathrm{T}} \approx 45$ GeV	0.1
	Energy scale	up to 200 GeV	0.3
	Reconstruction+ Identification efficiency (ID)	$P_{\mathrm{T}} \approx 45$ GeV	0.5
	Reconstruction+ ID+Isolation efficiency	$P_{\mathrm{T}} > 200$ GeV	2
Photon	Energy scale	$P_{\mathrm{T}} \approx 60$ GeV	0.3
	Energy scale	up to 200 GeV	0.5
	Resolution	$P_{\mathrm{T}} \approx 60$ GeV	10
	Reconstruction+ ID+Isolation efficiency	$P_{\mathrm{T}} < 200$ GeV	2
Jets	Absolute jet energy scale	—	1–2
	Pileup	—	0–2
	Jet flavour composition	—	0–0.5
	Jet flavour response	—	0–0.8
	b-jet efficiency	$30 < P_{\mathrm{T}} < 300$ GeV	1
	b-jet efficiency	$P_{\mathrm{T}} > 300$ GeV	2–6
	c-jet efficiency	all working points	2
	Light-jet mistag	working-point dependent	5–15

4.2. Kinematical cuts for discovery of excited electrons

In the signal–background analysis, we first applied the pre-selection cuts $P_{\mathrm{T}}^{e,\gamma,j} > 25$ GeV to the transverse momentum of the final-state particles, electron, photon, and jet in order to separate the excited electron signals from the background. We then obtained some kinematic distributions for both signal and background, and superimposed them on the same graph, so that we could compare the signal and the background. First, transverse momentum (P_{T}) and pseudorapidity (η) distributions for the final-state particles, electrons, photons, and jets of the ep collider with a center-of-mass energy of 8.44 TeV are plotted. In these distributions, mass values of $m_{e^\star} = 3900$, 5000, 6000, and 7000 GeV were used for the signal. Since the P_{T} and η distributions of the electron and photon are similar, only the distributions of the electron are given and these are shown in figure 5.

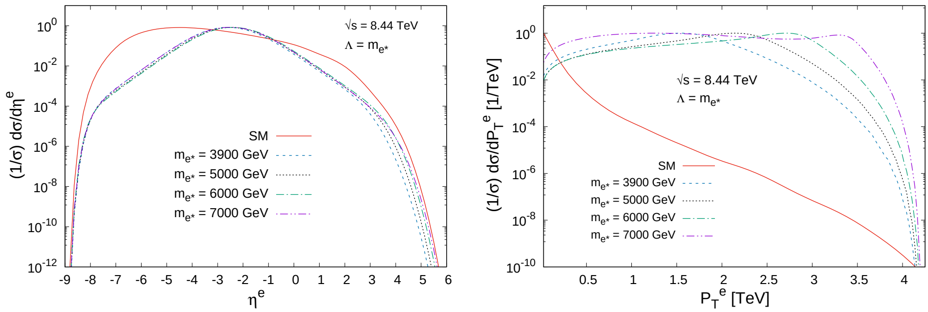

Fig. 5. The normalized pseudorapidity (left) and transverse momentum (right) distributions of the final-state electrons for the *ep* collider with a center-of-mass energy of 8.44 TeV.

Similar procedures were performed for the other *ep* colliders with center-of-mass energies of 11.66, 26.68, and 36.88 TeV, and the resulting distributions are shown in figures 6, 7, and 8, respectively.

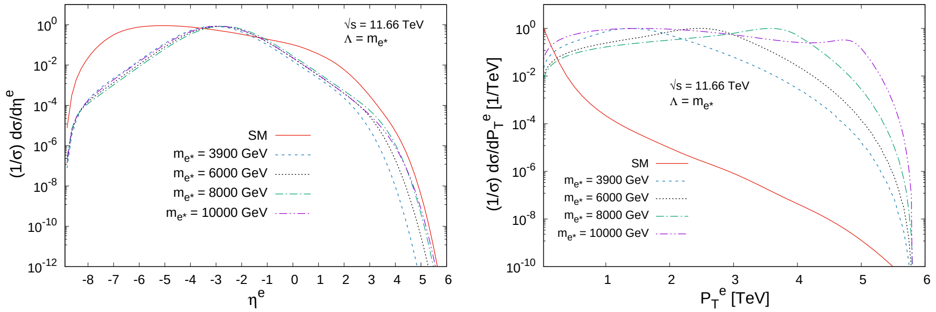

Fig. 6. The normalized pseudorapidity (left) and transverse momentum (right) distributions of the final-state electrons for the *ep* collider with a center-of-mass energy of 11.66 TeV.

When we examine the pseudorapidity plots of the final-state particles, it is clearly seen that these distributions peak in the negative region at all *ep* colliders. Considering that pseudorapidity is mathematically defined as $\eta = -\ln\tan(\theta/2)$, where θ is the polar angle, it is understood that electrons and photons are spatially backward, so we can say that excited electrons are mostly produced in the backward direction. This is mainly due to the asymmetric nature of the *ep* colliders. Since the energy of the electron is smaller, the pseudorapidity distributions are boosted towards the side from which the electron beam comes. Therefore, they peaked in the negative region.

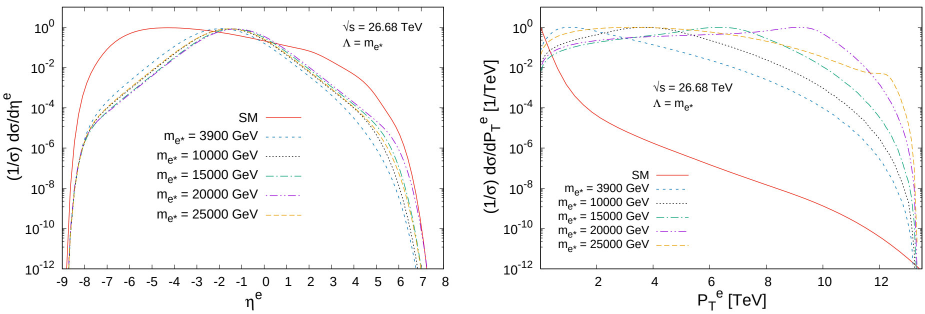

Fig. 7. The normalized pseudorapidity (left) and transverse momentum (right) distributions of the final-state electrons for the *ep* collider with a center-of-mass energy of 26.68 TeV.

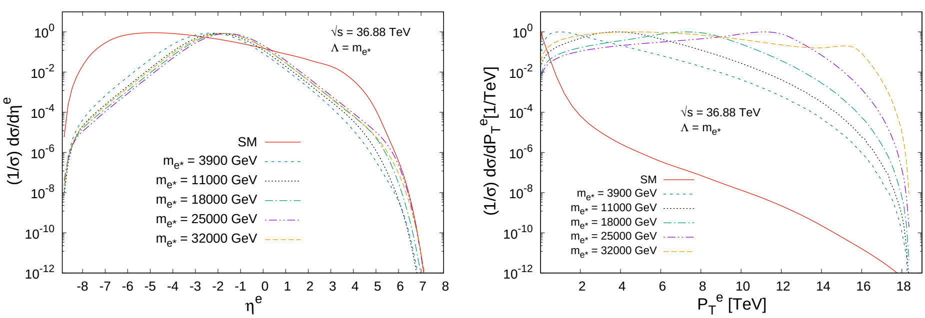

Fig. 8. The normalized pseudorapidity (left) and transverse momentum (right) distributions of the final-state electrons for the *ep* collider with a center-of-mass energy of 36.88 TeV.

On the other hand, when all P_{T} and η plots are analysed, it is seen that the signal and background distributions are slightly separated from each other. However, since the cross section of the background is larger, this separation is not sufficient to identify the signal from the background. Therefore, in addition to the pre-selection cuts, we need to apply large cuts, so-called discovery cuts. If we select regions $-3.5 < \eta^e < -0.5$ in the η plot and $P_{\mathrm{T}}^e > 500$ GeV in the P_{T} plots in figure 5, these cuts will hardly change the cross section of the signal. On the other hand, they will dramatically reduce the cross section of the background. A similar method was followed for the other P_{T} and η distributions, *i.e.* discovery cuts were determined so as not to affect the signal too much and to reduce the background. The determined discovery cuts for the P_{T} and η distributions of the particles of electron, photon, and jet in the final state are reported in Table 4. This table also shows the discovery cuts of the jets. However, their distribution plots are not given in this paper since the jets are not directly related to our signal.

Table 4. The discovery cuts in the P_{T} and η distributions of final-state particles at the SPPC-based *ep* colliders.

$\sqrt{s}$ [TeV]	p_{T}^{e} [GeV]	P_{T}^{γ} [GeV]	P_{T}^{j} [GeV]	η^{e}	η^{γ}	η^{j}
8.44	$P_{\mathrm{T}}^{e} > 500$	$P_{\mathrm{T}}^{\gamma} > 500$	$P_{\mathrm{T}}^{j} > 500$	$-3.5 < \eta^{e} < -0.5$	$-3.5 < \eta^{\gamma} < -0.5$	$-4 < \eta^{j} < 2.5$
11.66	$P_{\mathrm{T}}^{e} > 500$	$P_{\mathrm{T}}^{\gamma} > 500$	$P_{\mathrm{T}}^{j} > 500$	$-3.5 < \eta^{e} < -1$	$-3.5 < \eta^{\gamma} < -1$	$-4 < \eta^{j} < 2.5$
26.68	$P_{\mathrm{T}}^{e} > 500$	$P_{\mathrm{T}}^{\gamma} > 500$	$P_{\mathrm{T}}^{j} > 500$	$-2.5 < \eta^{e} < 0.5$	$-2.5 < \eta^{\gamma} < 0.5$	$-4 < \eta^{j} < 2.5$
36.88	$P_{\mathrm{T}}^{e} > 500$	$P_{\mathrm{T}}^{\gamma} > 500$	$P_{\mathrm{T}}^{j} > 500$	$-2.5 < \eta^{e} < 0$	$-2.5 < \eta^{\gamma} < 0$	$-4 < \eta^{j} < 2.5$

One of the most powerful methods to separate the signal from the background is to apply a cut to the electron–photon invariant mass distributions. The invariant mass distribution plots obtained after applying the pre-selection cuts are shown in figure 9. In these plots, it can be seen that the

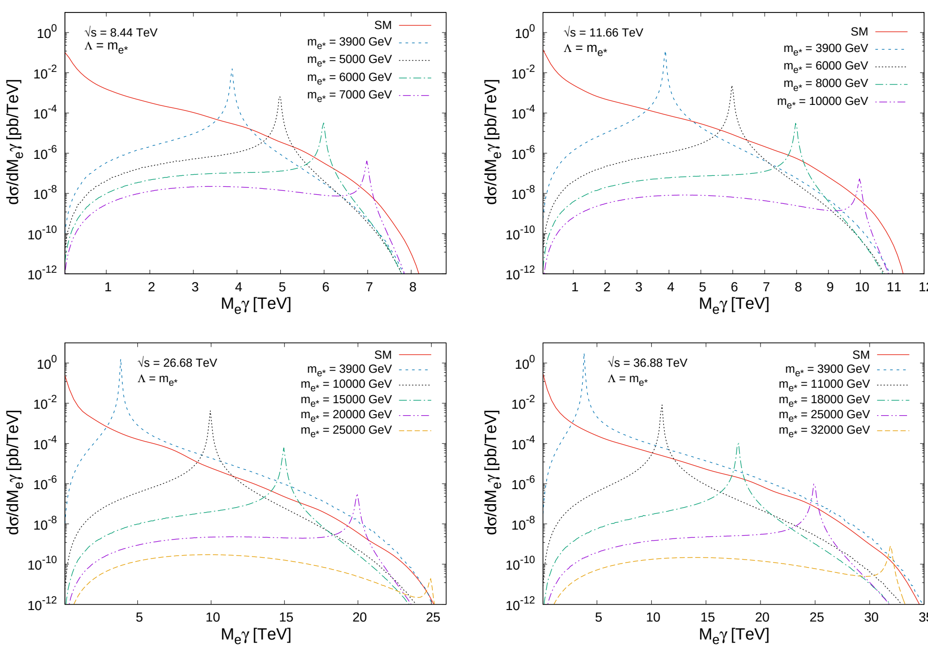

Fig. 9. The invariant mass distributions of the excited electron and corresponding background for the SPPC-based *ep* colliders.

line belonging to the background distribution is below the signal peaks. If we apply an invariant mass cut in the form of $m_{e^\star} - 2\Gamma_{e^\star} < m_{e\gamma} < m_{e^\star} + 2\Gamma_{e^\star}$, where Γ shows the decay width of the excited electron, we can make this line lower. The invariant mass cut is much more effective than the others, thus we also applied this effective cut.

In addition to the above-mentioned cuts, we applied some separation cuts in order to distinguish the final-state particles from each other. We applied the $\Delta R(e,\gamma) = 0.7$ [27] cut to separate the electron from the photon and the $\Delta R(j,\gamma) = \Delta R(j,e) = 0.4$ [29] cuts to separate the jets from the electron and photon. Here, ΔR is the separation cut and is defined as $\Delta R = \sqrt{\Delta\eta^2 + \Delta\phi^2}$.

4.3. Significance calculus

In the signal–background analysis, the discovery cuts mentioned in the previous subsection were used to separate the signal from the background and the Statistical Significance (SS) values of the expected signal yield were calculated. The following formula was used to calculate the SS values [52]:

$$\mathrm{SS} = \sqrt{2\left[(S+B)\ln\left(1+\left(\frac{S}{B}\right)\right) - S\right]}\,, \tag{13}$$

where S and B denote event numbers of the signal and background, respectively. Statistical errors are also included in these calculations. For this, the formula in equation (14), which is the version of equation (13) that includes potential systematic errors, is used [53]

$$\mathrm{SS} = \sqrt{2\left[(S+B)\ln\left(\frac{(S+B)\left(B+\sigma_{\mathrm{B}}^2\right)}{B^2+(S+B)\sigma_{\mathrm{B}}^2}\right) - \frac{B^2}{\sigma_{\mathrm{B}}^2}\ln\left(1+\frac{\sigma_{\mathrm{B}}^2 S}{B\left(B+\sigma_{\mathrm{B}}^2\right)}\right)\right]}\,. \tag{14}$$

In this formula, σ_{B} is the uncertainty in the background and is defined as $\sigma_{\mathrm{B}} = (\Delta B)B$. In the calculations, a total systematic uncertainty of 40% on average for all statistical errors on the background is taken into account [29]. Therefore, σ_{B} is taken as $\sigma_{\mathrm{B}} = 0.4\,B$. Using the data obtained as a result of the calculations, the variation graphs of the SS with respect to the mass of the excited electron were plotted. SS plots for all colliders are shown in figure 10.

Afterwards, more detailed calculations were performed to obtain the discovery (5σ), observation (3σ), and exclusion (2σ) values of the mass of the excited electron. According to the findings, the *ep* collider with a center-of-mass energy of 8.44 TeV will have the potential to discover excited electrons

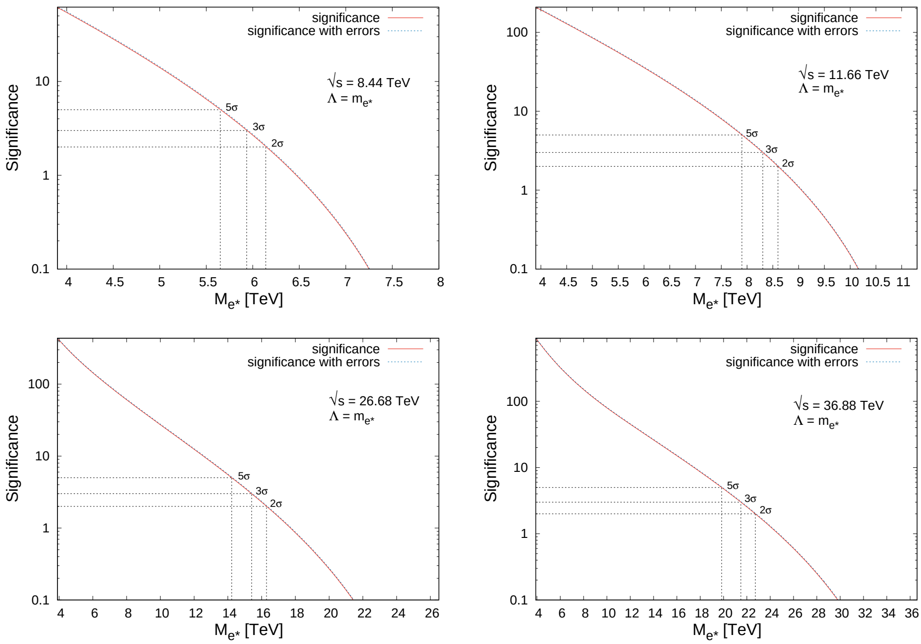

Fig. 10. Plots of the variation of statistical significance (SS) with respect to the mass of the excited electron at the SPPC-based *ep* colliders. The plots also include statistical errors.

up to mass $5650 \pm 2.32\%$ GeV, observe them up to a mass of $5935 \pm 2.37\%$ GeV, and exclude them up to a mass of $6140 \pm 2.44\%$ GeV. The mass limits obtained for all colliders are reported in Table 5.

Table 5. Attainable mass limits of the excited electrons for SPPC-based *ep* colliders.

$\sqrt{s}$ [TeV]	5σ [GeV]	3σ [GeV]	2σ [GeV]
8.44	$5650 \pm 2.32\%$	$5935 \pm 2.37\%$	$6140 \pm 2.44\%$
11.66	$7900 \pm 2.31\%$	$8305 \pm 2.37\%$	$8600 \pm 2.41\%$
26.68	$14230 \pm 2.27\%$	$15410 \pm 2.35\%$	$16290 \pm 2.42\%$
36.88	$19840 \pm 2.22\%$	$21485 \pm 2.30\%$	$22725 \pm 2.37\%$

In addition to these calculations, the highest compositeness scale values that can be achieved for each collider were calculated. The calculations show that as the mass of the excited electron increases, the compositeness scale values decrease inversely. Therefore, in order to reach the highest compositeness scale values, we should look for the smallest mass value. Considering that excited electrons are experimentally excluded up to 3.9 TeV, it would be appropriate to take the mass of the excited electron as 4 TeV for this calculation. Choosing the mass of the excited electron at 4 TeV, the values of the compositeness scale corresponding to 2σ, 3σ, and 5σ were calculated for each *ep* collider and the results are listed in Table 6. According to these results, the highest compositeness scale value can be reached at the collider with a center-of-mass energy of 36.88 TeV. At this collider, the compositeness scale for the discovery of the excited electron is $41915 \pm 3.63\%$ GeV.

Table 6. Attainable compositeness scale limits of the excited electrons with a mass of 4 TeV for the SPPC-based *ep* colliders.

$\sqrt{s}$ [TeV]	5σ [GeV]	3σ [GeV]	2σ [GeV]
8.44	$11800 \pm 3.74\%$	$14780 \pm 3.58\%$	$17625 \pm 3.96\%$
11.66	$21000 \pm 3.39\%$	$26200 \pm 4.32\%$	$31150 \pm 4.49\%$
26.68	$29830 \pm 3.54\%$	$37215 \pm 4.04\%$	$44210 \pm 4.54\%$
36.88	$41915 \pm 3.63\%$	$52260 \pm 4.16\%$	$62050 \pm 4.69\%$

4.4. Analysis of model-dependent uncertainties

Theoretical uncertainties in the cross-section calculations performed in the signal–background analysis arise from two main sources. The first of these is the errors originating from the PDF selection. Using different PDFs can give different results. In this regard, in Table 2, we simply compared the cross sections obtained from different PDFs for the signal process. However, we also need to analyse how different PDF sets affect the results. In this section, the signal–background analysis is repeated for different PDF sets in the *ep* collider with a center-of-mass energy of 8.44 TeV and the obtained results are compared. Since the use of different PDF distributions does not affect the discovery cuts, all the same cuts determined in the previous subsection are used in this analysis. The mass limits and achievable compositeness scale values obtained for different PDF distributions are reported in Tables 7 and 8, respectively.

The first column of these tables contains the names of the PDF distributions defined in the CalcHEP program, and the other columns contain the discovery (5σ), observation (3σ), and exclusion (2σ) mass limits, respectively. In the last row of the tables, the mean value of the mass limits and their standard deviations from this value are calculated. According to the obtained results, there is an uncertainty of 0.40%, 0.38%, and 0.52% in the

Table 7. Mass limits of excited electrons obtained for different PDF distributions in the *ep* collider with a center-of-mass energy of 8.44 TeV.

PDF	5σ [GeV]	3σ [GeV]	2σ [GeV]
CT10	5650	5935	6140
Cteq6l1	5685	5960	6165
NNPDF31_lo_as_0118	5710	6000	6230
PDF4LHC15_nlo_mc	5640	5930	6135
NNPDF23_lo_as_0130_qed	5675	5955	6160
NNPDF31_lo_as_0130	5675	5965	6185
Mean $\pm$ Standard deviation	5672.5 ± 22.87	5957.5 ± 22.87	6169.17 ± 31.81

Table 8. Compositeness scale limits of excited electrons obtained for different PDF distributions in the *ep* collider with a center-of-mass energy of 8.44 TeV.

PDF	5σ [GeV]	3σ [GeV]	2σ [GeV]
CT10	11800	14780	17625
Cteq6l1	12035	15060	17950
NNPDF31_lo_as_0118	11980	14990	17860
PDF4LHC15_nlo_mc	11805	14780	17620
NNPDF23_lo_as_0130_qed	11880	14870	17725
NNPDF31_lo_as_0130	11810	14780	17625
Mean $\pm$ Standard deviation	11885 ± 92.01	14876.67 ± 111.47	17734.17 ± 128.80

discovery, observation, and exclusion mass limits of the excited electron, as well as uncertainties of 0.77%, 0.75%, and 0.73% in the composition scale mass values, respectively.

The second of the theoretical uncertainties are the errors originating from renormalization (μ_{ren}) and factorization (μ_{fac}) scales. In the CalcHEP program, these two scale values are taken as equal to the invariant mass value ($M12$) of the two incoming particles (electron and proton in this study) as the default setting. This value has been used in the calculations made so far. In order to detect errors originating from renormalization and factorization scales, this scale value is usually changed in the range of 0.5–2 times around a central value. This process is done by taking the extreme values of this range and the error rate is determined by looking at the results. Therefore, in this analysis, the signal–background analysis was re-performed for half

($0.5 \times M12$) and twice ($2 \times M12$) of the $M12$ invariant mass value and the results were compared. The mass limits of the excited electron and the achievable compositeness scale values obtained for different renormalization and factorization scales are reported in Tables 9 and 10, respectively.

Table 9. Mass limits of excited electrons obtained for different renormalization and factorization scales in the *ep* collider with a center-of-mass energy of 8.44 TeV.

Scales	5σ [GeV]	3σ [GeV]	2σ [GeV]
$M12$	5650	5935	6140
$0.5 \times M12$	5680	5965	6170
$2 \times M12$	5625	5910	6120
Mean $\pm$ Standard deviation	5651.67 ± 22.48	5936.67 ± 22.49	6143.33 ± 20.55

Table 10. Compositeness scale limits of excited electrons obtained for different renormalization and factorization scales in the *ep* collider with a center-of-mass energy of 8.44 TeV.

Scales	5σ [GeV]	3σ [GeV]	2σ [GeV]
$M12$	11800	14780	17625
$0.5 \times M12$	12010	15030	17915
$2 \times M12$	11615	14535	17325
Mean $\pm$ Standard deviation	11808.33 ± 161.37	14781.67 ± 202.09	17621.67 ± 240.88

The tables show that the renormalization and factorization scale introduces errors of 0.40%, 0.38%, and 0.33% in the discovery, observation, and exclusion mass limits of excited electrons, respectively, with corresponding uncertainties of 1.37%, 1.36%, and 1.37% in the compositeness scale mass values.

5. Conclusion

In this study, we investigate the production of excited electrons by contact interactions and their decay into the photon channel by gauge interactions at the *ep* colliders. Calculations were performed for four different SPPC-based electron–proton colliders with center-of-mass energies of 8.44, 11.66, 26.68, and 36.88 TeV. In the signal–background analysis, in addition to pre-selection cuts, discovery cuts were applied to separate the excited electron signal from the background. In all calculations for the signal, the compositeness scale was taken equal to the mass of the excited electron. According to the results, excited electrons can be discovered up to $5650 \pm 2.32\%$

GeV at a collider with a center-of-mass energy of 8.44 TeV and an integrated luminosity of 251 pb^{-1}, and up to $7900 \pm 2.31\%$ GeV at a collider with a center-of-mass energy of 11.66 TeV and an integrated luminosity of 645 pb^{-1}. In the last two high-energy *ep* colliders, the collider with a center-of-mass energy of 26.68 TeV and an integrated luminosity of 73.7 pb^{-1} will be able to discover up to $14230 \pm 2.27\%$ GeV, and the collider with a center-of-mass energy of 36.88 TeV and an integrated luminosity of 189 pb^{-1} will be able to discover up to $19840 \pm 2.22\%$ GeV. In the next part of the study, the highest compositeness scale achievable at these colliders was investigated. Accordingly, excited electrons with a mass of 4 TeV can be discovered up to $11800 \pm 3.74\%$ GeV at the *ep* collider with a center-of-mass energy of 8.44 TeV, $21000 \pm 3.39\%$ GeV at the collider with a center-of-mass energy of 11.66 TeV, $29830 \pm 3.54\%$ GeV at the collider with a center-of-mass energy of 26.68 TeV, and $41915 \pm 3.63\%$ GeV at the collider with a center-of-mass energy of 36.88 TeV.

In the last part of the study, the error rates resulting from theoretical calculations for the *ep* collider with the lowest center-of-mass energy (8.44 TeV) were calculated. These errors were examined in two parts as errors originating from the selection of different PDF distribution functions and errors originating from the selection of renormalization and factorization scale. According to the results of the calculations, it was determined that the effect of these errors on the discovery, observation, exclusion mass limits of excited electrons and the highest compositeness scale values are very small. The highest error rate obtained is around 1%.

All these calculations for excited electrons show that the SPPC-based *ep* colliders will provide the possibility to scan a wide mass range for excited lepton searches. The observation of any excited lepton signal at these colliders will provide direct evidence for the existence of composite models.

I would like to thank Dr. M. Sahin from Usak University, Türkiye, for his support for the model file and for the useful consultations we had.

REFERENCES

[1] ATLAS Collaboration (G. Aad *et al.*), «Observation of a new particle in the search for the Standard Model Higgs boson with the ATLAS detector at the LHC», *Phys. Lett. B* **716**, 1 (2012).

[2] CMS Collaboration (S. Chatrchyan *et al.*), «Observation of a new boson at a mass of 125 GeV with the CMS experiment at the LHC», *Phys. Lett. B* **716**, 30 (2012).

[3] S. Weinberg, «Implications of dynamical symmetry breaking», *Phys. Rev. D* **13**, 974 (1976).

[4] L. Susskind, «Dynamics of spontaneous symmetry breaking in the Weinberg–Salam theory», *Phys. Rev. D* **20**, 2619 (1979).

[5] H. Georgi, S.L. Glashow, «Unity of All Elementary-Particle Forces», *Phys. Rev. Lett.* **32**, 438 (1974).

[6] J.C. Pati, A. Salam, «Lepton number as the fourth "color"», *Phys. Rev. D* **10**, 275 (1974).

[7] Y.A. Golfand, E.P. Likhttman, «Extension of the algebra of Poincare group generators and violation of P invariance», *JETP Lett.* **13**, 323 (1971).

[8] I.A. D'Souza, C.S. Kalman, «Preons: Models of Leptons, Quarks and Gauge Bosons as Composite Objects», *World Scientific*, 1992.

[9] H. Terazawa, Y. Chikashige, K. Akama, «Unified model of the Nambu–Jona-Lasinio type for all elementary-particle forces», *Phys. Rev. D* **15**, 480 (1977).

[10] H. Terazawa, «Subquark model of leptons and quarks», *Phys. Rev. D* **22**, 184 (1980).

[11] H. Terazawa, M. Yasuè, K. Akama, M. Hayashi, «Observable effects of the possible sub-structure of leptons and quarks», *Phys. Lett. B* **112**, 387 (1982).

[12] H. Terazawa, «A fundamental theory of composite particles and fields», *Phys. Lett. B* **133**, 57 (1983).

[13] H. Fritzsch, G. Mandelbaum, «Weak interactions as manifestations of the substructure of leptons and quarks», *Phys. Lett. B* **102**, 319 (1981).

[14] O.W. Greenberg, J. Sucher, «A quantum structure dynamic model of quarks, leptons, weak vector bosons and Higgs mesons», *Phys. Lett. B* **99**, 339 (1981).

[15] H. Harari, «A schematic model of quarks and leptons», *Phys. Lett. B* **86**, 83 (1979).

[16] M.A. Shupe, «A composite model of leptons and quarks», *Phys. Lett. B* **86**, 87 (1979).

[17] M. Sahin, A. Caliskan, «Excited muon production in muon colliders via contact interaction», *J. Phys. G: Nucl. Part. Phys.* **50**, 025002 (2023).

[18] A. Caliskan, «Search for Excited Muons at the Future SPPC-based Muon–Proton Colliders», *Acta Phys. Pol. B* **50**, 1409 (2019).

[19] A. Caliskan, S.O. Kara, «Single production of the excited electrons in the future FCC-based lepton–hadron colliders», *Int. J. Mod. Phys. A* **33**, 1850141 (2018).

[20] A. Caliskan, «Single production of the excited muons at the SPCC-based ultimate μp collider», *Turkish J. Phys.* **42**, 343 (2018).

[21] A. Caliskan, S.O. Kara, A. Ozansoy, «Excited muon searches at the FCC-based muon–hadron colliders», *Adv. High Energy Phys.* **2017**, 1540243 (2017).

[22] A. Caliskan, «Excited neutrino search potential of the FCC-based electron–hadron colliders», *Adv. High Energy Phys.* **2017**, 4726050 (2017).

[23] M. Sahin, G. Aydin, Y.O. Günaydin, «Excited quarks production at FCC and SppC pp Colliders», *Int. J. Mod. Phys. A* **34**, 1950169 (2019).

[24] A.N. Akay *et al.*, «Search for excited u and d quarks in dijet final states at future pp colliders», *Adv. High Energy Phys.* **2019**, 9090785 (2019).

[25] Y.O. Günaydin, M. Sahin, S. Sultansoy, «Resonance Production of Excited u Quark at FCC-based γp Colliders», *Acta Phys. Pol. B* **49**, 1763 (2018).

[26] A. Caliskan, «Single production of composite electrons at future SPPC-based lepton–hadron colliders», *Can. J. Phys.* **98**, 349 (2020).

[27] CMS Collaboration (A.M. Sirunyan *et al.*), «Search for excited leptons in $ll\gamma$ final states in proton–proton collisions at $\sqrt{s} = 13$ TeV», *J. High Energy Phys.* **2019**, 15 (2019).

[28] Particle Data Group (R.L. Workman *et al.*), «Review of Particle Physics», *Prog. Theor. Exp. Phys.* **2022**, 083C01 (2022).

[29] CMS Collaboration (A.M. Sirunyan *et al.*), «Search for an excited lepton that decays via a contact interaction to a lepton and two jets in proton–proton collisions at $\sqrt{s} = 13$ TeV», *J. High Energy Phys.* **2020**, 52 (2020).

[30] Y. Li, «CEPC Accelerator TDR Status Overview», «Proceedings of the 65$^{\mathrm{th}}$ ICFA Advanced Beam Dynamics Workshop on High Luminosity Circular e^+e^- Colliders (eeFACT'22)», Frascati, Italy, 12–16 September, 2022, pp. 14–18.

[31] J. Gao, «CEPC Accelerator TDR Status and AC Power Consumptions», «Proceedings of the 65$^{\mathrm{th}}$ ICFA Advanced Beam Dynamics Workshop on High Luminosity Circular e^+e^- Colliders (eeFACT'22)», Frascati, Italy, 12–16 September, 2022, pp. 262–269.

[32] CEPC Project Web Page, `http://cepc.ihep.ac.cn/intro.html`

[33] FCC Collaboration (A. Abada *et al.*), «FCC Physics Opportunities. Future Circular Collider Conceptual Design Report Volume 1», *Eur. Phys. J. C* **79**, 474 (2019).

[34] FCC Collaboration (A. Abada *et al.*), «FCC-ee: The Lepton Collider. Future Circular Collider Conceptual Design Report Volume 2», *Eur. Phys. J. Spec. Top.* **228**, 261 (2019).

[35] FCC Collaboration (A. Abada *et al.*), «FCC-hh: The Hadron Collider. Future Circular Collider Conceptual Design Report Volume 3», *Eur. Phys. J. Spec. Top.* **228**, 755 (2019).

[36] FCC Collaboration (A. Abada *et al.*), «HE-LHC: The High-Energy Large Hadron Collider. Future Circular Collider Conceptual Design Report Volume 4», *Eur. Phys. J. Spec. Top.* **228**, 1109 (2019).

[37] J. Tang, «Design Concept for a Future Super Proton–Proton Collider», *Front. Phys.* **10**, 828878 (2022).

[38] The CEPC-SPPC Study Group, CEPC-SPPC Preliminary Conceptual Design Report, Volume I — Physics & Detector, IHEP-CEPC-DR-2015-01, March, 2015.

[39] CEPC Study Group, «CEPC Conceptual Design Report: Volume 1 — Accelerator», arXiv:1809.00285 [physics.acc-ph].

[40] CEPC Study Group, «CEPC Conceptual Design Report: Volume 2 — Physics & Detector», arXiv:1811.10545 [hep-ex].

[41] Y. Zhang, Y. Peng, «A high energy e–p/A collider based on CepC-SppC», «Proceedings of the 6$^{\rm th}$ International Particle Accelerator Conference (IPAC2015)», *Jefferson Lab*, Richmond, VA, USA, 3–8 May, 2015.

[42] A.C. Canbay *et al.*, «SppC Based Energy Frontier Lepton–Proton Colliders: Luminosity and Physics», *Adv. High Energy Phys.* **2017**, 4021493 (2017).

[43] K. Hagiwara, D. Zeppenfeld, S. Komamiya, «Excited lepton production at LEP and HERA», *Z. Phys. C* **29**, 115 (1985).

[44] U. Baur, M. Spira, P.M. Zerwas, «Excited-quark and -lepton production at hadron colliders», *Phys. Rev. D* **42**, 815 (1990).

[45] A. Belyayev, N.D. Christensen, A. Pukhov, «CalcHEP 3.4 for collider physics within and beyond the Standard Model», *Comput. Phys. Commun.* **184**, 1729 (2013).

[46] A. Semenov, «LanHEP — A package for automatic generation of Feynman rules from the Lagrangian. Version 3.2», *Comput. Phys. Commun.* **201**, 167 (2016).

[47] J. Gao *et al.*, «Next-to-Leading QCD effect on the quark compositeness search at the LHC», *Phys. Rev. Lett.* **106**, 142001 (2011).

[48] CMS Collaboration (S. Chatrchyan *et al.*), «Search for contact interactions using the inclusive jet $p_{\rm T}$ spectrum in pp collisions at $\sqrt{s} = 7$ TeV», *Phys. Rev. D* **87**, 052017 (2013).

[49] H.L. Lai *et al.*, «New parton distributions for collider physics», *Phys. Rev. D* **82**, 074024 (2010).

[50] O. Aberle *et al.*, in: I. Béjar Alonso *et al.* (Eds.) «High-Luminosity Large Hadron Collider (HL-LHC) Technical Design Report», *CERN Yellow Reports: Monographs*, CERN, Geneva 2020.

[51] ATLAS Collaboration, «Expected performance of the ATLAS detector at the High-Luminosity LHC», ATLAS Pub Note, ATL-Phys-PUB-2019-005.

[52] G. Cowan, K. Cranmer, E. Gross, O. Vitells, «Asymptotic formulae for likelihood-based tests of new physics», *Eur. Phys. J. C* **71**, 1554 (2011).

[53] G. Cowan, «Discovery sensitivity for a counting experiment with background uncertainty», Technical Report, Royal Holloway, London, 2012.